Alex Wiens (Autor)

Tunable Ferroelectric Matching Networks implemented into High Power RF Amplifiers for High Dynamic and Wideband Efficiency

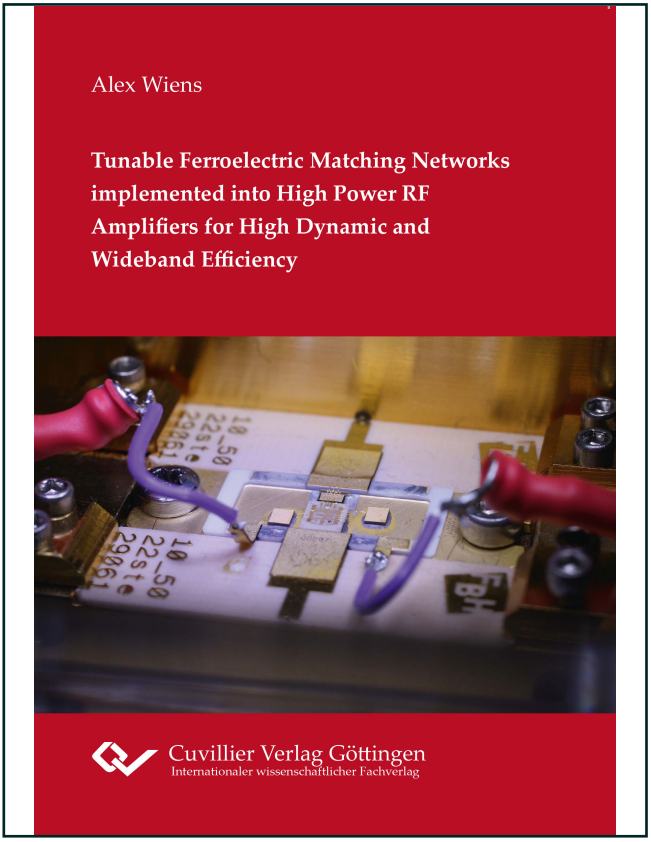

https://cuvillier.de/de/shop/publications/7505

1 Introduction

The continuous progress in modern wireless communication systems during the last decades is, and will be driven by the steadily increasing number of wireless devices and services. Beside the usual consumer electronics with the growing demand for broadband access to the internet, other upcoming fields such as *Industry 4.0* [Sch+15], *Internet of Things* (IoT) [Wor] as well as massively connected sensor networks [Com] are crowding the available frequency spectrum. Over the years, new bands have been allocated and advanced modulation schemes have been developed to cope with this circumstance. While adjusting the front end to the new requirements within the digital domain is rather straight forward, the analogue part of a transceiver can be considered as rigid, and therefore, the limiting factor of the whole wireless system. For example, the utilized filters and matching networks have an inherent trade-off between the achievable transmission and the bandwidth [Bod55], and are therefore, optimized to perform best in a certain, predefined frequency range. Especially in mobile devices, antennas play a significant role and are the focus of intense optimization to allow broadband operation (usually at the expense of matching). The amplifiers on the other hand are also limited in their application field, due to the inherent non-trivial matching problem. Deviation from the pre-defined operation scenarios (frequency, input power, temperature, etc.), usually leads to a drastic drop in performance and efficiency of the devices. Consequently, one of the key elements for multi band and multi standard operation is the possibility to adjust the analogue part of the RF front end by tuning the RF components.

To overcome the intrinsic physical limitations, which are partially addressed within this work, the implementation of modern transceivers is usually carried out in parallel trunks. Each branch is optimized to perform best at distinct standards within a certain, specified frequency band. However, this implementation suffers from the fact that only predefined standards and band as well as preequipped trunks can be used, which eventually leads to overaged transceivers, that need to be replaced. Further, the parallel implementation not only requires larger space and volume, but is also accompanied with an increased amount of components, which directly affects the costs. In case of active components, parallel implementation affects the

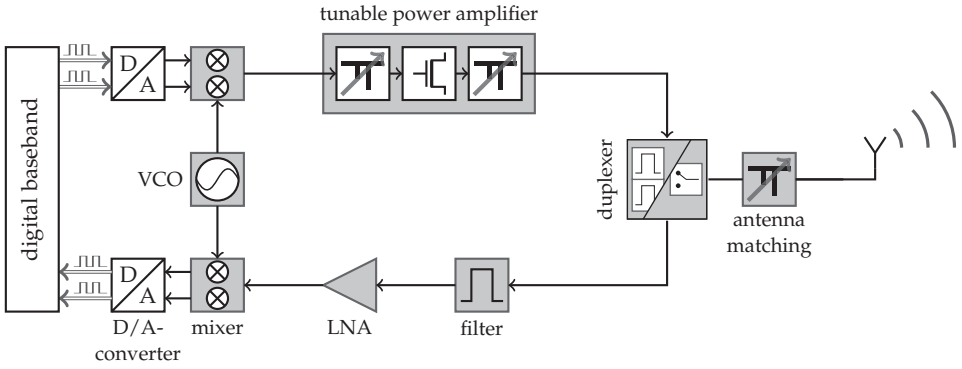

Figure 1.1: Concept of a fully reconfigurable RF front end in accordance to [Sch07a]. Gray-shaded blocks denote tunable elements such as matching networks, filters and other components.

overall power consumption, and hence, the efficiency. In the last consequence, this architecture requires isolated bands, which leave unused frequencies within the transitions from one band to another.

Especially the realization of *software defined radios* (SDR) and *cognitive radios* requires a completely reconfigurable analogue RF front end, which is not bound by predefined frequency bands and standards [Mit95; Mit00; PLL08]. First applications and devices, where exemplary the antenna's impedance is adjusted by tunable circuits have attracted attention [Gon+14]. Tunable filters, phase shifters and other components have been investigated and realized in various technologies for various operation frequencies [Gae+09; Zhe11; CC16]. However, the fully reconfigurable transceiver as depicted in Fig. 1.1 has not yet been deployed due to heterogeneous technologies, frequencies etc. Another important fact is that the energy efficiency, especially in handheld devices is one of the most critical requirements. In this context, the power amplifier (PA) of a transceiver system, unambiguously, can be considered as the main power consumer with around 70 % of the total transceiver's consumption [BZB10]. Depending on the operation class of the PA, large fraction of this energy is basically converted into heat (e.g. in class-A operation at least 50 %). The remaining portion is ideally the amplified signal, where the task is either to match over a wide frequency range and accept a reduced efficiency as a consequence of poor matching, or to reduce the bandwidth and tune the matching to achieve high efficiency. Consequently, the design and development of a tunable, efficient power amplifier is of utmost importance for energy efficient software defined radios.

The tunable elements of building blocks depicted in Fig. 1.1 can be fabricated implementing semiconductor varactor diodes, micro electromechanical systems (MEMS),

liquid crystals or ferroelectric tunable capacitors. Varactor diodes suffer from intrinsically low linearity and limited power handling capability for GHz RF applications, and hence have to be implemented in large arrays [Raa11] or can be only used in the receive path. MEMS offer good linearity and moderate power handling capability but suffer from mechanical fatigue [DSB08]. Liquid crystal based components have shown superior performance at frequencies above 10 GHz[Gae+09; Wei+13]. Ferroelectric ceramics such as KTN [Lau+05], BZT [XMI05] or BZN [Par+05] and many others have shown better performance below 10 GHz. Among them, especially ferroelectric varactors based on barium strontium titanate (BST) were found to have the most promising properties for the realization of tunable components at microwave frequencies [Tag+03; Gie09; Saz13].

The BST thick film technology offers a variety of benefits compared to other previously mentioned technologies. The material and the fabricated components offer sufficient and continuous tunability in combination with acceptable insertion loss below 10 GHz as well as good linearity. The material is inexpensive and allows the realization of all required building blocks for an SDR, especially in the high power path. Further, the bias voltage in combination with negligible leakage current allows powerless tuning, which has a direct impact on the efficiency of the system.

Within the last decade, individual tunable components for a fully reconfigurable RF front end based on BST have been demonstrated, including phase shifters [Gie+06; Ven07; Nik+14], filters [Nat+05; Sch16] and tunable impedance matching networks for antennas [Sch07b; Zhe11]. However, usually these components have only been tested under small signal conditions. First high power investigations have been conducted [Sch07a; Mau11] for inter-digital-capacitors (IDCs) and first tunable impedance matching networks have been investigated for high power transistors [Mau+12]. Nevertheless, the obtained efficiency and power handling capability of the fabricated components ($\geq$ 6 dB insertion loss) did not yield the expected improvements, which are necessary to advance the idea of a fully reconfigurable analogue RF front end.

The focus of this work is the systematic investigation of BST varactors for tunable impedance matching networks, compact enough to be implemented into the RF housing of a transistor. Especially the recently developed MIM varactors are examined for their suitability in high power applications.

Sophisticated numerical models for composite materials have been developed to allow CAD-aided prediction of dielectric properties and enable the design of novel, tailored materials.

Advanced numerical models of tunable components have been implemented and allow accurate prediction on tunability on a physical level and enable the extraction of key properties such as capacitance, resonance frequency as well as power handling capability. The designed models can be easily implemented in a circuit simulator and facilitate accurate prediction of tunable circuits behavior.

The proposed models are tested by two inherently different network synthesis methods, including filter theory design, and routes to consider tunable elements in the conventional (non-tuanble) filter synthesis. Further, a CAD-aided network synthesis method is proposed, which allows the synthesis of tunable circuits with exactly predefined characteristics.

2 Fundamentals of Nonlinear Dielectrics

2.1 Electric Polarization

A dielectric material is an electrical insulator that can be polarized by an externally applied electric field. When placed in an electric field, the charges, bound within the material, do not flow from one electrode to the other as they do in a conductor, but only slightly shift from their average equilibrium positions causing dielectric polarization $\vec{p}$, which is a measure of the separation of positive and negative electrical charges:

$$\vec{p} = q\vec{r} \quad , \tag{2.1}$$

with q being the charge and $\vec{r}$ being the distance of the charges. Considering a macroscopic volume, the effective (macroscopic) polarization can be obtained by summing up the individual microscopic polarizations $\vec{p}$:

$$\vec{P} = \sum_i \vec{p}_i / V \quad , \tag{2.2}$$

with V being the volume of the dielectric material. The polarization mechanisms can be subdivided depending on their origin:

- Space-charge polarization, where polarization occurs due to the diffusion of ions, along the field direction, thereby giving rise to redistribution of charges in the dielectrics.
- Orientation polarization, where molecules with built in dipole moments can independently rotate (and/or move) in an external electrical field.
- Ionic polarization, where ions in a lattice can be shifted from their equilibrium position by an external electrical field.

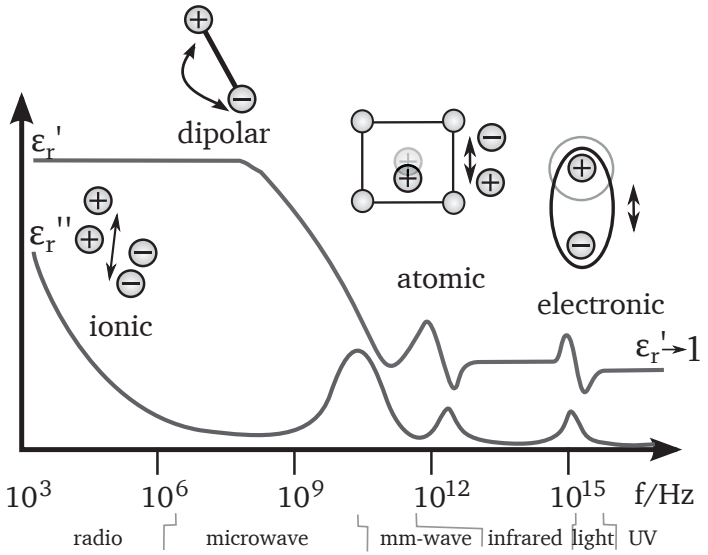

Figure 2.1: Qualitative frequency dependent real and imaginary part of the complex permittivity of a dielectric material, see (2.10).

- Electronic polarization, where the electrons, circling around an ion, are displaced from their average position with respect to the ion and, hence, create a dipole moment.

Depending on the frequency f of the external field $\vec{E}(f)$, the dominating mechanism is changing, due to different mass and mobility of the charges, as depicted in Fig. 2.1. In the simplest case[1], this phenomenon can be described as a mechanical spring-mass system, where the displacement $\vec{r}(t)$ of a charge can be written as:

$$\frac{q}{m_q}\vec{E}(t) - \frac{\delta^2}{\delta t^2}\vec{r}(t) - \Gamma\frac{\delta}{\delta t}\vec{r}(t) - \omega_0^2\vec{r}(t) = 0 \quad , \tag{2.3}$$

with m_q being the mass of the charge, ω_0 the resonance frequency of the movement and Γ the damping of the movement. In the case of a harmonic excitation (2.3) can be written as:

$$\frac{q}{m_q}\vec{E}(\omega) + \omega^2\vec{r}(\omega) - j\omega\Gamma\vec{r}(\omega) - \omega_0^2\vec{r}(\omega) = 0 \quad , \tag{2.4}$$

with the solution of the differential equation:

$$\vec{r}(\omega) = \frac{q}{m_q}\cdot\frac{\vec{E}(\omega)}{\omega_0^2 - \omega^2 + j\omega\Gamma} \quad . \tag{2.5}$$

[1] More advanced models have been developed by Cole-Cole [CC41] and Debye [Cof04]

And with (2.1) the polarization can be expressed as:

$$\vec{p}(\omega) = \frac{q^2}{m_q} \cdot \frac{\vec{E}(\omega)}{\omega_0^2 - \omega^2 + j\omega\Gamma} \quad . \tag{2.6}$$

Using the relation between the displacement field $\vec{D}$ and the electric field:

$$\vec{D} = \underline{\varepsilon}\vec{E} = \varepsilon_0\vec{E} + \vec{p} \quad , \tag{2.7}$$

a complex permittivity $\underline{\varepsilon}$ can be defined:

$$\underline{\varepsilon} = \varepsilon_0 \left(1 + \frac{q^2}{\varepsilon_0 m_q} \cdot \frac{1}{\omega_0^2 - \omega^2 + j\omega\Gamma}\right) = \varepsilon' - j\varepsilon'' \quad , \tag{2.8}$$

where the imaginary part can be seen as dissipated energy and the real part can be considered as stored energy within the dielectric in the form of electrical field. Consequently, the ratio of both, can be used as a measure to characterize the quality of the material.

$$\tan\delta = \frac{\varepsilon''}{\varepsilon'} = \frac{1}{Q} \quad , \tag{2.9}$$

where Q is referred to a quality factor of a dielectric.

$$\underline{\varepsilon} = \varepsilon' - j\varepsilon'' = \varepsilon'\left(1 - j\tan\delta\right) = \varepsilon_0\varepsilon_r\left(1 - j\tan\delta\right) \quad . \tag{2.10}$$

However, in absence of an external electrical field $\vec{E}$, most dielectric materials have randomly oriented dipole moments summing up to $\vec{P} = 0$. Ferroelectrics, on the other hand, belong to a sub-class of dielectrics, which allow the preservation of an internal polarization. The properties of this material class is the focus of the following section.

2.2 Perovskite Ferroelectrics

Ferroelectrics obtained their name due to their phenomenological accordance to ferromagnetics, which maintain their magnetic moments, once oriented in an external magnetic field. In a similar manner, the ferroelectric materials maintain a reminiscent macroscopic polarization P_R in the absence of an external electrical field. This effect is also often referred to as a *hysteresis* in polarization. Fig. 2.2 shows a qualitative polarization of a ferroelectric material versus external electrical field. In the

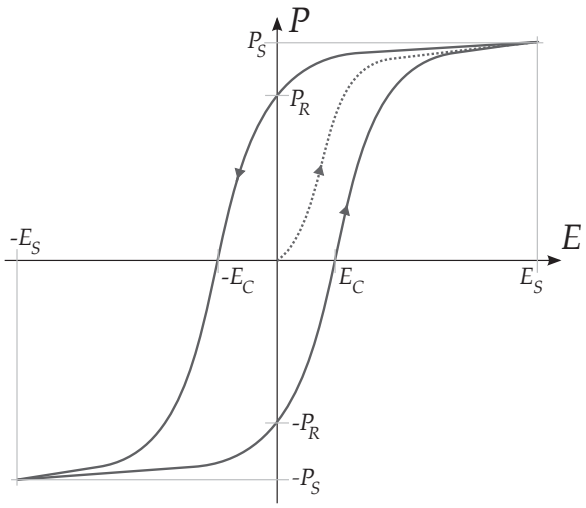

Figure 2.2: Qualitative characteristics of a ferroelectric polarization versus the external field.

initial state (red curve), the dipole moments $\vec{p}$ of the material are randomly oriented summing up to $\vec{P} = 0$. Application of an external field aligns the dipole moments until a saturation polarization P_S at a saturation field strength E_S is reached. After reducing the external field to $E = 0$, a certain reminiscent polarization P_R remains. The field has to be reversed to a value E_C to obtain $\vec{P} = 0$. Numerous ferroelectrics are found in a so called Perovskite structure, with the general formula of ABO_3. In this structure, an A-site ion, on the corners of the lattice, is usually an alkaline earth or rare earth element. The center of the lattice is occupied by B-site ions and can be 3d, 4d, and 5d transition metal elements. This material class distinguishes itself by a characteristic transition between a ferroelectric phase in a tetrahedral- and a paraelectric phase in a cubic lattice structure [Pau06]. Depending on the materials, this transition occurs at a distinct temperature called Curie temperature T_C. At this point, the permittivity ε' reaches a maximum. Fig. 2.3 qualitatively shows this transition, which can be thermodynamically described by the Ginzburg-Landau-Theory [GS01].

The nonlinear response of P manifests the E-field dependency of the relative permittivity:

$$\varepsilon_r = \frac{1}{\varepsilon_0}\frac{\partial P}{\partial E} \quad . \tag{2.11}$$

For the realization of tunable components, a paraelectric phase is preferred, as in this phase a memory effect of the polarization is avoided (or reduced). Usually

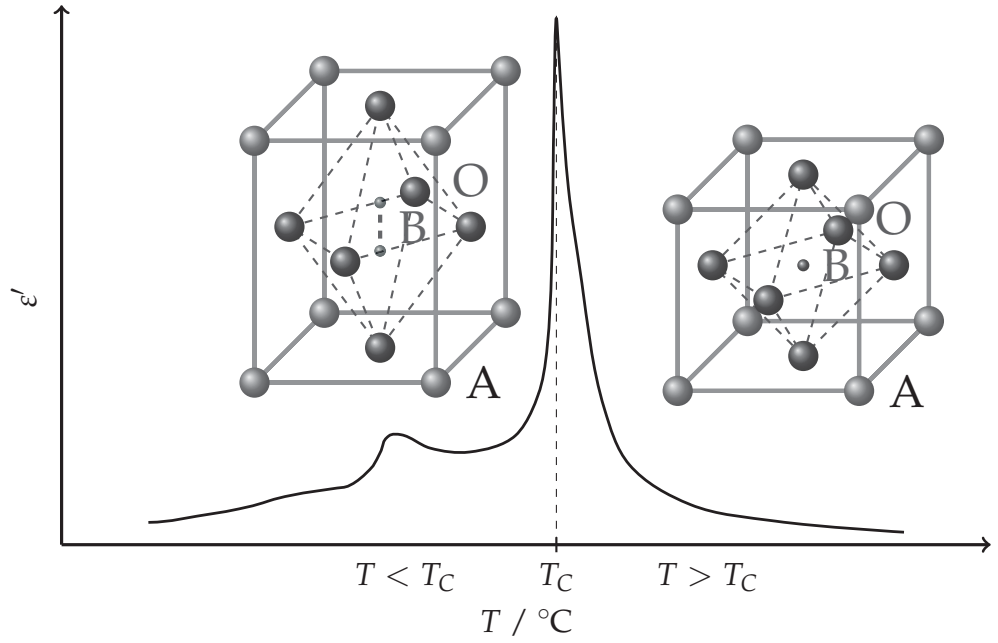

Figure 2.3: Qualitative characteristic of a Perovskite ferroelectrics versus temperature with a distinct transition from ferroelectric to paraelectric phase at the Curie temperature T_C. The inset shows a tetrahedral and cubic lattice structure without external bias fields. The axes are randomly scaled.

the material is operated closely above the Curie temperature T_C to maintain large electric tunability:

$$\tau(E) = \frac{\varepsilon_r(E=0) - \varepsilon_r(E)}{\varepsilon_r(E=0)} \quad , \tag{2.12}$$

where E is the electric field. For tunable varactors (2.12) is less convenient and rewritten as capacitances:

$$\tau(U_B) = \frac{C(U_B=0) - C(U_B)}{C(U_B=0)} \quad , \tag{2.13}$$

where U_B is the applied bias voltage. However, at the Curie temperature, not only the tunability τ is highest but also the dielectric losses of the material $\tan\delta$. Therefore, the choice of the material system and the operation temperature are of importance. There are also applications below Curie temperature, where the memory effect of the polarization is used to store information, such as *FeRAM* [Zhe11; Sco07].

However, for the work here, the paraelectric phase of the ferroelectric materials is of predominant interest.

One of the most prominent ferroelectric materials for microwave applications is barium strontium titanate (BST) with barium or strontium as the at the A-site ions and titanium as the B-site ion [Gev09]. In the following, the focus is put on its fabrication, processing, dielectric properties and modeling.

2.3 Barium Strontium Titanate

Commercial devices are usually operated in a temperature range between 0 °C and 50 °C. Hence, the Curie temperature of the tunable material should be below or around the lower temperature limit to keep the paraelectric phase throughout the desired temperature range. So far, no pure ferroelectric material with Perovskite structure is known that has a Curie temperature of approximately 0 °C. Therefore, polycrystalline materials are synthesized, where the phase transition from ferroelectric to paraelectric is adjusted by the amount of the constituents. Pure barium titanate ($BaTiO_3$) has a transition temperature at around $T_{C,BaTiO_3} \approx 105\,°C$, which can be reduced by an admixture of strontium titanate ($SrTiO_3$) with a transition temperature of $T_{C,SrTiO_3} \approx -250\,°C$ [Tag+03]. In this mixture, the Sr ions substitute the Ba ions at the A-site. The result is a polycrystalline Perovskite ferroelectric $Ba_xSr_{1-x}TiO_3$, where the Curie temperature can be adjusted by the stoichiometric factor $x \in \{0..1\}$. Other rare earths can be combined in a similar manner to adjust the transition temperature but with inferior properties at microwave frequency range [Lau+05; XMI05; Par+05; Pau06]. Fig. 2.4 shows the permittivity ε_r versus temperature for different stoichiometric compositions x of bulk ceramic materials, measured at 1 kHz [Jeo04]. With increasing Ba fraction T_C is shifted towards higher temperatures. At the same time the permittivity is decreasing. For single crystal and bulk ceramic materials, the transition temperature T_C can be approximated as [Tag+03]:

$$\begin{aligned} T_{C,s}(x) &= -244.8 + 368.3x - 18.58x^2\,[°C]\,, && \text{Single crystal} \\ T_{C,c}(x) &= -240.9 + 485.6x - 136.8x^2\,[°C]\,, && \text{Ceramic} \end{aligned} \tag{2.14}$$

The single crystal shows a nearly linear dependence between x and the resulting Curie temperature, while bulk ceramics show increased cubic dependence. The effect can be attributed to defects within the material. According to (2.14), a Curie temperature around 0 °C is obtained with $x = 0.6$, which is in good agreement with reported measurement results [Jeo04; Tag+03]. Consequently, the material is